Journal of Thermal Analysis and Calorimetry, Vol. 70 (2002) 277–290

IDENTIFICATION OF MICRO-SCALE CALORIMETRIC DEVICES II
Heat transfer models from two- or three-dimensional analysis

*C. Auguet, F. Martorell, F. Moll and V. Torra**

CIRG-DFA-ETSECCPB, Polytechnical University of Catalonia, C/. Gran Capità s/n, Campus Nord B-4, E-08034 Barcelona, Spain

Abstract

The miniaturized calorimetric devices furnish a reduced working flat surface and permits measurements with extremely low-mass quantities. The experimental sensitivity shows relevant position dependence with *x*-*y* surface coordinates and with *z*-distance. The device identification is realized via a 2-D model based in Fourier general equation. Using the Marquardt method the experimental flat surface device can be identified and the fitted parameters used to simulate the behavior of the experimental system. From the model, the effects of several dissipation configurations can be evaluated. Also, via the RC-analogy, a way to 3-D experimental devices is roughly described.

Keywords: accuracy, conduction calorimeters, identification, models, shape factor

Introduction

The first heat conduction calorimeter (Tian calorimeter) was introduced around 1920 [1]. Calvet progressively improved the experimental device. After 1956, with the publication of the Calvet book [2], the system became a commercial device. In fact, D.A.M. Company became a calorimetric manufacturer in 1960. The first criticisms concerning the accuracy of the results (not the reproducibility) are well documented in Colloquia (in Marseilles) realized in 1965 and published in 1967 [3]. Several manufacturers have developed diverse types of progressively automated instruments until today. At present, conduction calorimeters are broadly used for characterizing materials.

Accurate or traceable measurements to the Joule effect or other well-known standard measurements (i.e. the combustion of benzoic acid, the benzene-cyclohexane mixture or the dilution of KCl solution in water) are subjects of permanent interest in conduction calorimeters. In particular when the accurate measurements is the main target. Today, the authoritative arguments of Calvet [discussion in [3] (pp. 329–339)] remain in actual computerized devices: ‘The same total area will al-

* Author for correspondence: E-mail: vtorra@fa.upc.es

1418–2874/2002/ $ 5.00

Akadémiai Kiadó, Budapest
Kluwer Academic Publishers, Dordrecht

ways be obtained independently of the type of thermogram or the distortions occasioned by the variations of the position in the cell's interior, ... what changes is the form according to the position of the thermal source within the interior of the cell. The effect is important in thermokinetics but in calorimetry it is irrelevant....'. The experimental effects of these arguments are highly relevant in current devices (isothermal or programmed). The difficulties are old and intrinsic, also in standard melting processes. Pessimistic observations are, also, present in the discussion (realized in 1965). In page 289 of [3], Kleppa indicates: '... Some years ago we carried out some experiments … However, we abandoned these experiments in favor of isothermal methods, due to difficulties of calibration. We believe the non-isothermal method is not to be recommended for purely thermodynamic work. On other hand it offers interesting possibilities in the study of rate problems.'

We could consider as a consequence of Colloquia 1965 [3] that the authoritative arguments established that, at constant temperature, the sensitivity of the devices was invariant. This situation has practically remained for the 35 following years until the present time. It is only supposed that the sensitivity is a function of temperature. In [4] Callanan explains the main difficulties encountered on temperature determination and, also, on fusion enthalpy measurements: 'Instruments classified as differential scanning calorimeters (DSC) and differential thermal analyzers (DTA) require the use of correction procedures in order to measure the thermal properties accurately'. But using a heating rate of 10 K min^{-1}, the direct measurement of Al melting temperature scatter from 927.2 to 929.4 K using strictly the manufacturer software (thermodynamic value 933.61 K). The fusion enthalpy scatters from 312.4 to 326.3 J g^{-1}, but the standard value is 370.0 J g^{-1}. In relative analysis the differences are not important, but the systematic error on melting enthalpy overcomes 15 per cent. In fact, some misunderstanding between accurate and reproducible measurements is relatively classic in conduction calorimeters [5] and, is expected an increase in reliability via more sophisticated models [6]. Last year an international measurement program is launched in isothermal as in temperature programmed expecting an increase in accuracy on the measurements. In temperature induced, basically realized in a conventional Differential Scanning Calorimeter 2910 MDSC, TA Instruments [7]. The results show relevant positional differences on the sensitivity. Using samples with relatively lower thermal conductivity the sensitivity differences can approach 40 per cent [8].

Today, the instruments center on two associate targets. The first one relates the particular and home-made devices built for energetic and specific measurements. For instance, the device described in [9, 10] is built to determine the energy balance in hydrogen absorption in an open system. The analysis of positional dissipation realized in [9, 10] is not complete to ensure the reliability of the energetic results. Using an axial heater in the working cell furnishes reproducible results but does not explain the eventual differences related to radial positioning, i.e. using heaters of cylindrical shape with different diameter. Using several heaters with cylindrical shape in the same cell the coaxial effects are visualized [11].

The second one, using manufactured DSC devices, is associated to more qualitative interests, i.e. in [12–13] the target relates the evaluation and the advantages of

several materials in hydrogen storage. The main interest relates the search of relevant changes on temperature peaks position associated with hydrogen desorption.

Recently, the study of extremely low quantity of mass is realized via miniaturized devices [14–18]. Recently, reliable (as reproducible) results are obtained using silicon based devices with Al–Si detectors. Several devices based in Si-based chip (i.e. LCM 2524 [19] or similar liquid nano calorimeter) are built to analyze gas composition using gas-solid host-guest reactions. In liquids, the mixing enthalpy can be evaluated via drop to drop reactions or, in steady state, using a chamber with continuous inflow and outflow of liquid mixtures. Via experimental measurements, a shape factor in two or three dimensions is suggested to reduce the systematic error [7].

In this work, the behavior of the flat Si device is experimentally studied and a two-dimensional model, based in Fourier equation, is built. Using a Marquardt approach [20], the model parameters are determined from experimental measurements. The model permits an identification of the device and their simulation and, for instance, an evaluation of the shape factor; i.e., the simulation permits an evaluation of the dissipation position effects. In fact, the model is a necessary tool to estimate what is the more appropriate experimental configuration.

Experimental set-up

The experimental analysis is realized determining the positioning effect of the dissipation. The experimental setup is schematically described in Fig. 1. In experimental analysis the warmed signal is a laser pointer (Fig. 1 left). The resolution and reproducibility of the laser spot position is close to 0.5 mm. Figure 1 right shows a general outline of the experimental system in positioning analysis. The schematic character-

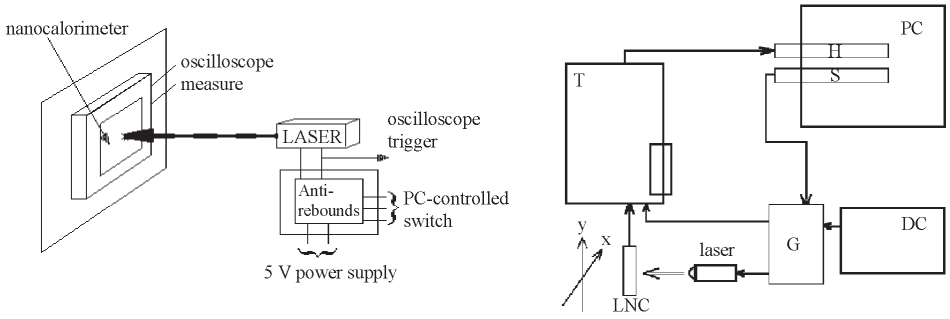

Fig. 1 Experimental-setup. Left: Schematic device: laser and calorimetric working surface. Right: Outline of the complete device; T: oscilloscope Tektronik TDS 420; DC: power supply (PREMIUM SR-120) for laser and electronic gates; G: gates (signal to oscilloscope and power supplied to laser); S: switch interface card; H: GPIB interface card; laser: wavelength 645 nm, power <5 mW, EDMUND (L54-006) [21]. LNC: liquid nano calorimeter (XENSOR, model LCM 2524), *x-y* coordinates: positioning the LNC via two orthogonal turn devices EDMUND (L-38531); PC: old 386 PC

istics of the silicon device, in particular the thermocouples position (forming a squared frame), is represented in Fig. 2 left.

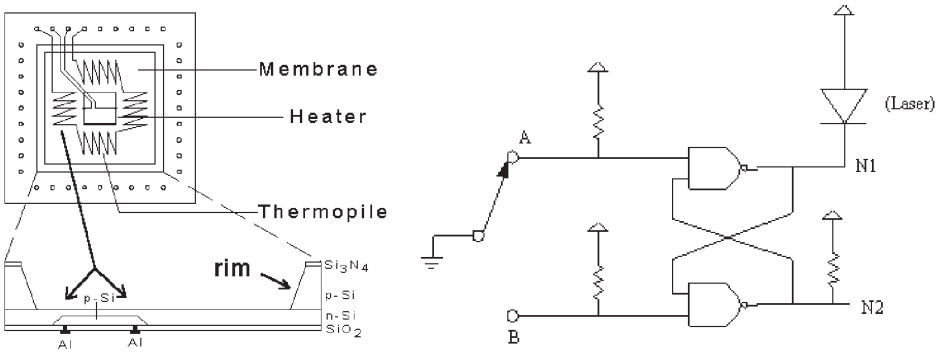

Fig. 2 Left: Schematic distribution of the LCM 2524 (rear part). Silicon thickness: working surface 25 μm, rim 1 mm. Right: Circuit to avoid mechanical rebounds caused by the relay (see text)

The input signal or 'thermogenesis' (a thermal stimulus) is applied with a cheaper laser-pointer, which is switched 'on' and 'off' by two relays (PC controlled). In order to avoid mechanical rebounds inherent to these kinds of switches, a small circuit controls the laser power supply. This circuit is shown in Fig. 2 right and it consists of two cross-coupled open-collector NAND logic circuits (one 7438 chip). One of the relays (relay A) allows a connection between terminal A and ground, and the second relay (relay B) either connects or disconnects terminal B to the ground. When relay B is ON and relay A is OFF, node N2 is at the TTL 'V' Voltage (nominal value 5 V) which, together with node A at 'V' due to its pull-up resistor, cause a low voltage (close to 0 V) at node N1, turning the laser on. When relay A is ON and relay B is OFF, N1 is at 'V', which turns the laser off, while N2 is close to 0 V. Node N2 is used to trigger the oscilloscope, starting the measurement when the laser is switched off (transition high to low in node N2). When both A and B are disconnected, which can happen because of mechanical rebounds, N1 and N2 do not change from their previous value, and thus the laser is immune to mechanical rebounds. The situation in which both relays A and B are ON should be avoided. The same power supply furnishes power to laser and to the circuit. In the measurements, the TTL 'V' voltage is appropriately reduced and 2.823 V are commonly used.

In each run the digital oscilloscope captures several series of measurements. Each series of measurements (an acquirement) represents the response to several squared signals (up to 200) acting on the laser (on: 6 s; off: 16 s). A little delay (close to 10 μs) is observed between the laser cut-off and the initial disappearance of the output signal (Fig. 3). The starting point of the capture relates the stop point of the la-

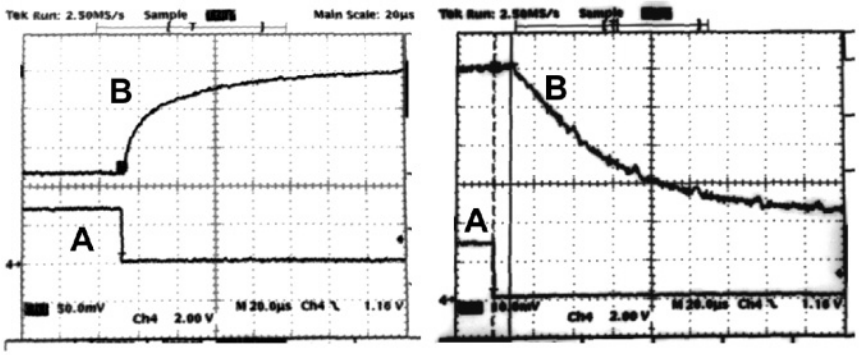

Fig. 3 Time delay between the laser cut-off (A) and the photon-electron disappearance (B) for 'negative' and 'positive' photon-electron signal. The photon-electron signal, positive or negative and position dependent overcome 150 mV. The thermal signal induced by the same laser spot remains under 2.5 mV

ser signal (a Heaviside decay) with a minor delay (2.5 ms) to avoid the parasitic photon-electron effects. The oscilloscope realizes the mean value and stores them. Each series of measurements is separately stored in computer RAM-disk. For each run, a visual analysis of each acquirement permits that the unexpected noisy measurements can be suppressed and, also, to determine the mean response of each run.

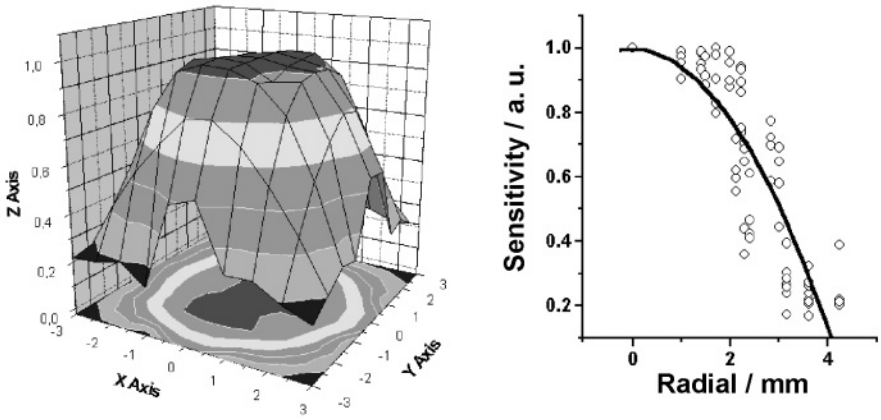

Fig. 4 Left: Free chip device: sensitivity changes in relative units *vs*. *x*-*y* coordinates. Right: relative values in radial representation. Continuous line: second order radial fit to all *x*-*y* experimental measurements

The used digitizing sampling is 0.0004 s and 15000 points are stored. Usually, each studied measurement depicts 4000 acquisitions to smooth the noise and the low digitizing resolution (only one byte) used by the oscilloscope.

Experimental results

The sensitivity is determined from the extrapolation to the origin (t=0) of the Heaviside return. Using the laser spot, with unknown fraction of absorbed power, the relative curves and the relative sensitivity are established. For it, all points of the output signals are divided by the steady signal in the center of the liquid-nano calorimeter surface. The relative sensitivity decays with the distance to the center with a squared symmetry (close to a cylinder symmetry). In Fig. 4 (left), the relative sensitivity determined from the laser spot is represented *vs*. the x-y coordinates. Figure 4 (right) shows the relevant scatter partly associated to the squared effects in a radial representation. In fact, using only a radial representation [7], the sensitivity scatter is relevant and the reliability is relatively poor. A careful representation of the sensitivity values requires the x, y coordinates, for instance, using one representation as S=S(x, y).

The 2-D model

A first approach determines the behavior of the squared silicon surface: a perfectly flat surface with irrelevant thickness (Δz). The parasitic effect related to Al wires and silicon oxide used in manufacturer heater and in the other wires is considered irrelevant. Using appropriate thermal losses in the geometrical borders and in the upper and lower surface the representation can be analyzed via the Fourier equation. Using only a two-dimensional description and including, in z-axis, a direct heat flux to surrounding, the corresponding Fourier equation reads

$$\alpha\Delta T+w/(\rho c)=\partial T/\partial t+P^* T \tag{1}$$

In the equation, Δ represents the two-dimensional Laplace operator, α is the 'mean' thermal diffusion in the working space, $w(x, y, t)$ is the dissipated power density (in W m^{-3}), ρc the density times the heat mass capacity and P^* is for the apparent thermal coupling with the surroundings in z-axis – top and bottom surfaces – (P^*=P_z/($\rho c\Delta z$)).

General solution

When the heat dissipation is zero (w=0), the general solution reads

$$T(x, y, t)=A\cos(\omega_x x+\phi_x)\cos(\omega_y y+\phi_y)e^{-at} \tag{2}$$

The differential equation establishes the link between the parameter a (related to the relaxation time scale) and the ω_x and ω_y by:

$$a=\alpha(\omega_x^2+\omega_y^2)+P^* \tag{3}$$

The heat transfer to the surroundings establishes four boundary conditions:
At x boundaries is accomplished:

$$x=0,\ y\in[0,\ \ell_y]\quad -P_x T_{x=0}=-k(\partial T/\partial x)_{x=0} \tag{4-1}$$

$$x=\ell_x,\ y\in[0,\ \ell_y]\ \ -k(\partial T/\partial x)_{x=\ell_x}=P_x T_{x=\ell_x} \tag{4-2}$$

Applying the general form of $T(x, y, t)$, Eq. (4-1) reads

$$-P_x A\cos(\phi_x)\cos(\omega_y y+\phi_y)e^{-at}=+k\omega_x A\sin(\phi_x)\cos(\omega_y y+\phi_y)e^{-at}$$

or
$$-P_x\cos(\phi_x)=+k\omega_x\sin(\phi_x) \tag{4-1'}$$

Using (4-2)

$$+k\omega_x A\sin(\omega_x\ell_x+\phi_x)\cos(\omega_y y+\phi_y)\ e^{-at}=P_x A\cos(\omega_x\ell_x+\phi_x)\cos(\omega_y y+\phi_y)\ e^{-at}$$

or
$$+k\omega_x\sin(\omega_x\ell_x+\phi_x)=P_x\cos(\omega_x\ell_x+\phi_x) \tag{4-2'}$$

Combining (4-1') and (4-2') the transcendent equation for ω_x can be deduced:

$$(P_x^2-k^2\omega_x^2)\sin\omega_x\ell_x+2P_x k\omega_x\cos\omega_x\ell_x=0 \tag{4-2"}$$

and, for each ω_x, the ϕ_x value will be determined using Eq. (4-1'). Similar conditions are defined at y boundaries and equivalent transcendent equations furnish the values for ω_y and ϕ_y.

Using the solutions of transcendent equations, Eq. (3) provides the time constants ($\tau_{ij}=1/a_{ij}$) via

$$a_{ij}\equiv a(i,j)=\alpha(\omega_x(i)^2+\omega_y(j)^2)+P^* \tag{5}$$

as it can be seen from this expression the dynamic system response is explicitly function on thermal diffusion and vertical losses.

The action of the double infinite series of $\omega_x(i)$ and $\omega_y(j)$ (or ω_i and ω_j) with their associate values of phases $\phi_x(i)$ and $\phi_y(j)$ (or ϕ_j and ϕ_j) converts the general solution in the form:

$$T(x, y, t)=\Sigma_{ij}A_{ij}\cos(\omega_i x+\phi_i)\cos(\omega_j y+\phi_j)\exp(-a_{ij}t) \tag{6}$$

Coefficients: Dirac dissipation in a circular region

Once the general solution is obtained the effect of the dissipation ($w(x, y, t)$) is calculated through orthogonalization of the temperature distribution at t=0. In order to simplify the notation we define the coefficients B

$$B(\omega_i,\ \phi_i,\ \omega_j,\ \phi_j)=\iint\cos^2(\omega_i x+\phi_i)\cos^2(\omega_j y+\phi_j)\,dx\,dy$$

The integral can be calculated and B value, for each pair of i and j index, can be written as:

$$B_{ij}=(1/4)\ [\ell_x+(1/2\omega_i)\ \{\sin2(\omega_i\ell_x+\phi_i)-\sin2\phi_i\}]\ [\ell_y+(1/2\omega_j)\{\sin2(\omega_j\ell_y+\phi_j)-\sin2\phi_j\}]$$

A_{ij} coefficients can be determined as:

$$A_{ij}(\delta)=\iint T(x, y, t=0)\cos(\omega_i x+\phi_i)\cos(\omega_j y+\phi_j)\,dx\,dy/B_{ij} \tag{7}$$

In squared device $\ell_x=\ell_y$ and $P_x=P_y$, and matrix A is symmetric $A_{ij}=A_{ji}$.

The laser spot can be roughly modeled as a circular area. The dissipation, a pulse of 1 *J*, determines a temperature step ΔT^C as

$$\Delta T^C=1\ J/(\rho c\ \pi r^2\ \Delta z)$$

A_{ij} value established by the integral extended to the heated surface (formula 7) can be rewritten in the actual dissipation geometry –a Dirac pulse in a circle– by the A^C_{ij} as:

$$A^C_{ij}=\iint T(x, y, t=0)\cos(\omega_i x+\phi_i)\cos(\omega_j y+\phi_j)\,dx\,dy/B_{ij}=$$

$$=\Delta T^C\iint_C\cos(\omega_i x+\phi_i)\cos(\omega_j y+\phi_j)\,dx\,dy/B_{ij}$$

A new coordinate origin (to the circle center), and several new coefficients (A_1 and B_1) facilitates an approach to the calculus. Using an *x*-*y* representation the solution can be represented by a sine and cosine series but a mixture of square and circle is difficult. To avoid complex development a rough approximation permits a first step in the evaluation of the integral value (V_C). Using the values at the inner square (value V_I and area a_I) and the outer square (value V_O and area a_O) surrounding the circle (value V_C and area a_C), V_C value reads

$$V_C=V_I+(a_C-a_I)\ (V_O-V_I)/(a_O-a_I)$$

a^* and a^{**} (and a_I and a_O) are defined by

$$a^*=r/(2)^{0.5}\quad a_I=(2a^*)^2=2r^2$$

$$a^{**}=r\quad a_O=4r^2$$

V_O and V_I are:

$$V_I=(4/\omega_i\omega_j)\ A_1B_1\ \sin\omega_i a^*\ \sin\omega_j a^*$$

$$V_O=(4/\omega_i\omega_j)\ A_1B_1\ \sin\omega_i a^{**}\ \sin\omega_j a^{**}$$

So A_{ij} coefficients for the circular Dirac pulse reads as

$$A_{ij}=\Delta T^C\ (V_I+(a_C-a_I)\ (V_O-V_I)/(a_O-a_I))$$

Heaviside dissipation

The coefficients A_{ij}(H) associate to an 'on' Heaviside signal (a positive step signal) are:

$$A_{ij}(\mathrm{H})=\int_0^\infty A_{ij}(\delta)\,dt=A_{ij}(\delta)/a_{ij}$$

The temperature dependence reads

$$T(x, y, t)=\Sigma_{ij}A_{ij}(\mathrm{H})\cos(\omega_i x+\phi_i)\cos(\omega_j y+\phi_j)\ [1-\exp(-a_{ij}t)]$$

In steady state $T(x, y, t=\infty)$ value is:

$$T(x, y, t=\infty)=\Sigma_{i\,j}A_{i\,j}(\mathrm{H})\cos(\omega_i x+\phi_i)\cos(\omega_j y+\phi_j)$$

The temperature dependence after the Heaviside step reads

$$T(x, y, t)=\Sigma_{ij}A_{ij}(\mathrm{H})\cos(\omega_i x+\phi_i)\cos(\omega_j y+\phi_j)\exp(-a_{i\,j}t)$$

Sensor response model

At last, a model describing the experimental detector unit is necessary: a thermocouple array that provides the voltage output. The output depends on the average difference between the internal and external sides. Defining T_I and T_E as the mean inner temperature (warmer junctions) and the mean external temperature (cold junctions) and using k_S as the Seebeck effect coefficient, the thermocouple output $s_\delta(t)$ related to a Heaviside input signal can be modeled via

$$s_\delta(t)=k_S(T_I-T_E)$$

The mean temperature T_I, integrated on the four-sided square determined by the warmed junctions (total length $\ell_I=2(\ell_x-2b+\ell_y-2b)$ reads

$$T_I=[1/\ell_I]\int_I \Sigma_{ij}A_{ij}(\mathrm{H})\cos(\omega_i x+\phi_i)\cos(\omega_j y+\phi_j)\exp(-a_{i\,j}t)\,\mathrm{d}\ell=$$
$$=[1/\ell_I]\,\Sigma_{ij}A_{ij}(\mathrm{H})\exp(-a_{i\,j}t)\int_I\cos(\omega_i x+\phi_i)\cos(\omega_j y+\phi_j)\,\mathrm{d}\ell \qquad (8)$$

T_E, related to the colder junctions (total length $\ell_E=2(\ell_x-2a+\ell_y-2a)$ reads

$$T_E=[1/\ell_E]\,\Sigma_{ij}A_{ij}(\mathrm{H})\exp(-a_{i\,j}t)\int_E\cos(\omega_i x+\phi_i)\cos(\omega_j y+\phi_j)\,\mathrm{d}\ell \qquad (9)$$

The integrals $\int_I$ and $\int_E$ can be calculated. After integration, the time dependence is explicit and the positional effects of the laser impact on x_0, y_0 remains implicit in the formalism. In a general form, the output or calculated signal after a cut-off in the Heaviside signal can be written via

$$s_\delta(t)=k_S\,\Sigma_{ij}\,A^*_{ij}\exp(-a_{i\,j}t)$$

In A^*_{ij} value the dissipation position (the x_0, y_0 coordinates) are included. From their definition

$$A^*_{ij}=A_{ij}(\mathrm{H})\,\{C^I_{ij}-C^E_{ij}\}$$

Coefficients C^I_{ij} and C^E_{ij} can be calculated from T_I and T_E [22].

Fit between the experimental and the simulated response

The approach to physical parameters describing the two-dimensional device is realized via fitting of experimental data: an adapted Marquardt method has been used. The method (a non-linear fit), estimates the dependence of the squared error (differ-

ence between experimental and calculated points) with each researched parameter (a_i). a_i represents the 'free' parameters to be fitted, i.e. the thermal diffusion, the heat losses, the time delay, and so on. The original algorithm is based on the estimation of the changes on the diagonal of the Hessian matrix (α_{ij}) via the infinitesimal changes (δa_i) on the parameters. To avoid an excessive variation on the parameters, induced by the Hessian coefficients value (inverse-Hessian method in [20]), a new coefficient (λ) is introduced [22]

$$\alpha'_{jj}=\alpha_{jj}\ (1+\lambda)$$

$$\alpha'_{ij}=\alpha_{ij}\ (i\neq j)$$

Modifying λ the algorithm can switch between steepest descent and inverse-Hessian method as α' matrix approach to α matrix (the diagonal dominant matrix). Changing from α_{jj} to α'_{ij} and using the β_k as the derivatives of the error against the unknown parameters, the inverse-Hessian method is modified as

$$\sum_l \alpha'_{kl}\ \delta a_l=\beta_k$$

Marquardt method is a classical method in nonlinear fitting. In identifying calorimetric devices it is important to take into account some particular considerations. Variation on parameters is governed by derivatives and the functions used in fitting can present difficulties. In the numerical analysis careful attention is always necessary. Furthermore, as variation relies on derivative values it can go to minimal values without physical relevance. So it is useful to define a range of possible physical values and to consider a maximum amount of variation for each step. As the algorithm relies on a least-square method, it is necessary to use the more relevant experimental data, the appropriate parameter values on the first iteration and only one group of parameters for each partial path of approximation. In fact, the iterative method uses Marquardt as a formal support for several steps of a semi-quantitative approach [23–24].

For fitting process data has been prepared as:

I) Removal of the offset from the data series. Each series has a different offset value (or the asymptotic value in base line) due to non-differential effects. The formal model is based on a series of exponential terms decaying to zero and the offset value should be removed previously to the Marquardt fit.

II) Normalization of the data set using the central point of the chip in time 2.5 ms (start of measurements after decaying the photon-electron effects).

III) Smoothing the data. To reduce the effects of noise data has been partially smoothed.

IV) Selection of points to fit. For each *x*-*y* coordinate, only 16 points are selected from 15000 available. A selection of the relevant points for the fitting process is necessary.

In the presented analysis, only five positions are analyzed and, practically, the fit is realized only varying the thermal diffusion. Table 1 contains the starting points used for the fitted parameters. In the used approach only the thermal diffusion is analyzed. Figure 5 left shows the experimental output associated to a return of Heaviside

signal and the simulated signals are compared. The mean differences do not overcome 0.3 per cent.

Table 1 Thermal and mechanical parameters of the flat silicon surface. Initial values and fitted values used in the 2-D approach

Parameter	Starting value	Fitted value	Units
Px	$296.0 \cdot 10^{5}$	–	W m^{-2} K^{-1}
Py	$296.0 \cdot 10^{5}$	–	W m^{-2} K^{-1}
Pz	8.0	–	W m^{-2} K^{-1}
Lx	$8.7 \cdot 10^{-3}$	–	m
Ly	$8.7 \cdot 10^{-3}$	–	m
K	148.0	–	W m^{-1} K^{-1}
ρ	$2.57 \cdot 10^{3}$	–	kg m^{-3}
C	705.0	–	J kg K^{-1}
Δ*z*	$25.0 \cdot 10^{-6}$	–	m
A	$4.3 \cdot 10^{-3}$	–	m
b	$1.9 \cdot 10^{-3}$	–	m
r	$0.3 \cdot 10^{-3}$	–	m
Δ*t*	$0.1 \cdot 10^{-4}$	–	s
α	$81.685 \cdot 10^{-6}$	$99.5 \cdot 10^{-6}$	m^2 s^{-1}

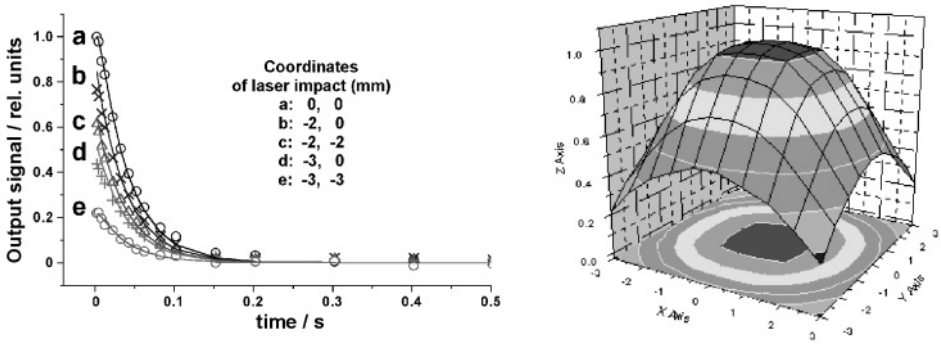

Fig. 5 Left: Experimental Heaviside return for different laser spot position. Experimental values: o, x, +, Δ. Fitted values: continuous line. The laser spot position (mm) is referred to the center of the silicon surface. Right: relative sensitivity. Calculated values using the results of the Marquardt fit

Evaluation of the positioning effects

In the experimental devices the working space (or the reaction space) determines a dissipation surface. The model permits an evaluation of the global surface effects and

the associate shape factor. For instance, Table 2 shows several examples of the calculated sensitivity using a constant power density. In particular, one centered square of 2×2 mm^2, one centered square of 3.4×3.4 mm^2, a rectangular and centered surface of 3.0×0.6 mm^2 close to the projection of a Pt resistance in liquid mixtures by continuous injection [18], a frame as the manufacturer's resistance (Fig. 2 left) and a square of 8.7×8.7 mm^2 corresponding at the complete silicon surface. The shape factor (*SF*) is evaluated, for each dissipation, dividing the calculated sensitivity by the value in the simulated manufacturer resistance. The calculated sensitivity and the shape factor behavior are coherent with the output signal decrease associated with the mean dissipation position. When part of the dissipation is situated between the warm junctions and the external border (I+O in Table 2) the sensitivity decreases. Other surface shapes or power densities are possible via their decomposition in 'elementary squares' and appropriate addition. Obviously, the treatment permits the analysis of inhomogeneous power density; i.e. as the expected dissipation using a continuous liquid mixture entering by only one inlet and close the silicon surface [25].

Table 2 Calculated sensitivity values (in model units: K W^{-1}) and associated shape factors in the 2-D model. Inside: inside of the warmed thermocouple junctions. Outside: out of the square determined by the warmed junctions

Inside (I) Outside (O)	Simulated heater: shape and position	Calculated sensitivity/ K W^{-1}	Shape factor
I	square centered 2.0×2.0 mm^2	26.792	1.006
I	square centered 3.4×3.4 mm^2	26.691	1.002
I+O	square centered 5.5×5.5 mm^2	22.841	0.857
I+O	square centered 6.5×6.5 mm^2	19.515	0.733
I+O	square centered 8.7×8.7 mm^2	12.460	0.468
I	frame (manufacturer resistance) surface near 4×(3.4–2.9)×3.4 mm^2	26.643	1
I	Rectangular centered 3.0×0.6 mm^2	26.861	1.008

A preliminary formal approach to 3-D analysis

The actual available computer possibilities in identification and data processing are more important and cheaper in comparison with the numeric possibilities in the related subjects realized in the eighties [23–24, 26–27]. The decomposition of a 3-D system in N finite domains at uniform temperature T_j [6], with C_j heat capacities and P_{jk} thermal couplings and external surrounding temperature T_0, permits a treatment via a system of linear differential equations:

$$W_j = C_j \frac{dT_j}{dt} + \sum_{k \neq j} P_{jk}(T_j - T_k) + P_j(T_j - T_0);\ j = 1, 2, \ldots, N$$

Using N elements it is possible to build a model similar to a structure in 3-D as, for instance, a drop on the working surface. In the drop surface some heat losses need to be introduced and, obviously, the sensitivity (or detected signal) is related to the heat fraction between the detected heat *vs.* the heat lost [6–7]. This ratio depends on the relative position of the dissipated heat: more close to warm junctions or more close to the external surroundings [7–8, 28]. Using an elementary RC-model equivalent to a cylindrical device (only *r* and *z* coordinates) the *z*-coordinate effects can be easily recognized [6, 28]. In a formal way, from the experimental measurements an identification of the thermal parameters via modified Marquardt algorithm is possible [23–24].

Conclusions

The conduction calorimeter started by Tian in the twenties. In the sixties, the appearance of a metrology problem is recognized. Today, the reproducibility is excellent but the guaranteed accuracy remains a partially unsolved problem. The experimental and the theoretical analysis, carried out by means of models based on Fourier equation, clearly establishes the dissipation position effect on sensitivity. The difference between the dissipation geometry in calibration and in actual measurements induces relevant systematic errors. One recent approach relates the modification of the standard sensitivity (method furnished by the equipment manufacturer) via a shape factor associated to the true positional effects of the actual dissipation.

The behavior of the flat Si device is experimentally and theoretically studied. A two-dimensional model, based in Fourier equation, is built. An approach to model parameters is realized from experimental measurements using a modified Marquardt algorithm. From the model and for each configuration, the shape factor can be determined by simulation. The model permits the simulation of the experimental device and an evaluation of the positional effects in the dissipation. In other words, the model is a tool to estimate more appropriate experimental configuration of the reaction cell or, eventually, what the expected fluctuation margins in the energetic results are.

* * *

The ACES 1999-00040 (Gen. of Catalonia) related to nanocalorimeters and fruitful discussion with Dr. J. Lerchner from Freiberg group are gratefully acknowledged. Part of this work is carried out in the frame of integrated actions HA 1999-0087 (MCT-Spain) between Freiberg/Sachsen (FRG) and Barcelona group and the ACI99-2 (Gen. Cat.) between Barcelona with Marseilles (France). The historical hints on conduction calorimeters suggested by Prof. H. Tachoire from Marseilles group are acknowledged.

References

1 A. Tian, Recherches sur la calorimétrie par compensation. Emploi des effets Peltier et Joule. Étude d'un microcalorimètre intégrateur, oscillographe et balistique, L. Jean, Imprimeur, Gap, 1933.

2 E. Calvet and H. Prat, Microcalorimétrie, Masson 1956.

3 Microcalorimétrie et Thermogenèse, n° 156, Éditions du Centre National de la Recherche Scientifique, Paris 1967.
4 J. E. Callanan, J. Thermal Anal., 45 (1995) 359.
5 V. Torra and H. Tachoire, Thermochim. Acta, 203 (1992) 419.
6 V. Torra and H. Tachoire, J. Therm. Anal. Cal., 52 (1998) 663.
7 V. Torra, C. Auguet, J. Lerchner, P. Marinelli and H. Tachoire, J. Therm. Anal. Cal., 66 (2001) 255.
8 P. Marinelli, J. Lerchner and V. Torra, unpublished results obtained in Differential Scanning Calorimeter 2910 MDSC, TA Instruments, (August, 2001).
9 P. Dantzer and P. Millet, Thermochim. Acta, 370 (2001) 1.
10 P. Dantzer and P. Millet, Rev. Sci. Instrum., 71 (2000) 142.
11 E. Cesari, PhD, Faculty of Physics, University of Barcelona, Spain 1978.
12 F. C. Gennari, F. J. Castro and G. Urretavizcaya, J. Alloys and Compounds, 321 (2001) 46.
13 F. C. Gennari, F. J. Castro and J. J. Andrade Gamboa, Synthesis of Mg_2FeH_6 by reactive mechanical alloying: formation and decomposition properties, preprint (CAB-Argentina 2001).
14 J. Lerchner, D. Caspary and G. Wolf, Sens. Actuators B, 70 (2000) 57.
15 J. Lerchner, A. Wolf and G. Wolf, J. Therm. Anal. Cal., 57 (1999) 241.
16 J. Lerchner, A. Wolf, A. Weber, R. Hüttl and G. Wolf, in 'Microreaction Technology: Industrial Prospects', Ed. W. Ehrfeld, Springer 2000, p. 469.
17 A. Wolf, A. Weber, R. Hüttl, J. Lerchner and G. Wolf, Thermochim. Acta, 337 (1999) 27.
18 J. Lerchner, A. Wolf, A. Weber, R. Hüttl, G. Wolf, J. M. Köhler and M. Zieren, On-line monitoring of Enzyme Activities using Microreactor Heat Power meters, Proc. of 3th International Conference on Microreaction Technology, Frankfurt/Main, Germany, 1999.
19 Liquid micro calorimeter by Xensor Integration, Delft, The Netherlands (www.xensor.nl).
20 W. H. Press, S. A. Teukolsky, W. T. Vetterling and B. P. Flannery, Numerical Recipes in Fortran, Cambridge University Press, 2nd ed. 1992.
21 EDMUND Industrial Optics, catalog 2001 (www.edmundoptics.com).
22 Detailed formalism on source listing can be obtained from the authors.
23 C. Auguet, J. Lerchner, V. Torra and G. Wolf, J. Therm. Anal. Cal., in preparation (2001).
24 H. Tachoire, J. L. Macqueron and V. Torra, Signal processing in microcalorimetry: applications on thermodynamics and kinetics, 105 (1986) 333. (in French).
25 H. Tachoire and V. Torra, Thermochim. Acta, 110 (1987) 171.
26 M. Rodriguez de Rivera, F. Socorro, J. P. Dubes, H. Tachoire and V. Torra, Thermochim. Acta, 150 (1989) 11 (in French).
27 F. Socorro, M. Rodriguez de Rivera, J. P. Dubes, H. Tachoire and V. Torra, Meas. Sci. Technol., 1 (1990) 1285 (in French).
28 J. Lerchner, G. Wolf, C. Auguet and V. Torra, Thermochim. Acta, in preparation.